

pubs.acs.org/JPCB Article

Structural Features and Nonlinear Rheology of Self-Assembled Networks of Cross-Linked Semiflexible Polymers

Published as part of The Journal of Physical Chemistry virtual special issue "Jose Onuchic Festschrift". Saamiya Syed, Fred C. MacKintosh, and Jordan L. Shivers*



Cite This: J. Phys. Chem. B 2022, 126, 10741-10749



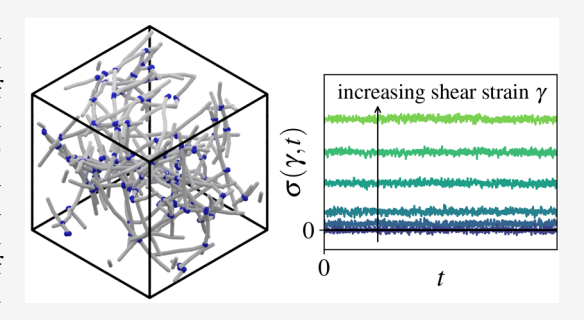
ACCESS I

III Metrics & More

Article Recommendations

S Supporting Information

ABSTRACT: Disordered networks of semiflexible filaments are common support structures in biology. Familiar examples include fibrous matrices in blood clots, bacterial biofilms, and essential components of cells and tissues of plants, animals, and fungi. Despite the ubiquity of these networks in biomaterials, we have only a limited understanding of the relationship between their structural features and their highly strain-sensitive mechanical properties. In this work, we perform simulations of three-dimensional networks produced by the irreversible formation of cross-links between linker-decorated semiflexible filaments. We characterize the structure of networks formed by a simple diffusion-dependent assembly process and measure their associated steady-state rheological features at finite temperature



over a range of applied prestrains that encompass the strain-stiffening transition. We quantify the dependence of network connectivity on cross-linker availability and detail the associated connectivity dependence of both linear elasticity and nonlinear strain-stiffening behavior, drawing comparisons with prior experimental measurements of the cross-linker concentration-dependent elasticity of actin gels.

1. INTRODUCTION

The formation of living things involves the energy-intensive assembly of complex structures from scarce resources. Survival requires that these structures remain robust and functional under significant and often repetitive applied stresses and strains. Quasi-one-dimensional or filamentous structures address these challenges efficiently by supporting significant tensile stresses with minimal material cost. Biological polymers and fibers are generally also semiflexible, meaning that they resist modes of deformation that induce bending, such as applied compression. In examples spanning a wide range of length scales, including information-storing DNA and RNA, actin and intermediate filaments in the cell cytoskeleton, and extracellular collagen and elastin fibers in tissues, these mechanical features are essential for biological function.

The cytoskeleton and extracellular matrix are examples of disordered networks, a common class of higher order structures in living materials. Building on the qualities of their underlying semiflexible filaments, these networks act as responsive elastic scaffolds that resist extreme deformation while leaving ample space for the transport and storage of functional components, such as interstitial fluids and cells. Unlike conventional elastic solids, their mechanical properties are scale dependent^{3,4} and sensitive to changes in applied stress or strain,^{5–7} to which they respond with dramatic stiffening, alignment, and changes in local filament density, enabling essential biological phenomena such as long-range force

transmission by cells⁸⁻¹² and muscle fiber contraction. ^{13,14} Recent work has suggested that the nonlinear viscoelastic properties of these and related fibrous networks are governed by an underlying mechanical phase transition associated with the onset of stretching-dominated rigidity under applied shear or extensile strains. Within this framework, elastic properties are predicted to exhibit a power-law dependence on applied strain in the vicinity of a critical strain, and nonaffine (inhomogeneous) rearrangements that become increasingly large near the critical strain are expected to drive a significant slowing of stress-relaxation as the transition is approached.¹⁷ This slowing occurs due to the physical coupling of the rearranging elastic network to a viscous background (the solvent) and is closely related to the well-known divergence of the viscosity of dense particulate suspensions near the onset of jamming. 18,19 The magnitude of the critical strain, at which these effects are the most pronounced, depends sensitively on key features of the underlying network architecture. 20,21

Received: August 1, 2022 Revised: November 18, 2022 Published: December 7, 2022





Extensive simulation-based studies have explored the nonlinear rheological properties of disordered networks of cross-linked stiff or semiflexible polymers, 5,22-24 in some cases with realistic three-dimensional geometries produced by either physical assembly processes 12,25-31 or artificial generation procedures.^{32–37} However, efforts to specifically connect network structure with strain-controlled critical behavior have typically focused on simplified random spring networks. $^{16,20,38-46}$ In spring networks, the critical strain coincident with the onset of stretching-dominated mechanics can be tuned by changing the average connectivity z, defined as the average number of bonds joined at each network junction. 20 For a network of cross-linked filaments, z is controlled by the typical number of cross-links formed per filament, approaching an upper limit of $z \rightarrow 4$ at high crosslinking density.²¹ In biopolymer gels, small changes in the concentration of available cross-linkers can drive dramatic changes in rheological properties,⁴⁷ including changes in the linear elastic modulus⁴⁸ and shifts in the critical strain corresponding to the onset of stretching-dominated mechanics. 49 These changes are naively consistent with a tendency of the connectivity to increase with cross-linker concentration. However, the quantitative relationships between cross-linker concentration, connectivity, and the structural characteristics of assembled networks more generally, have remained poorly understood. Improving our knowledge of how the concentration-dependent microscopic structural details of selfassembled networks translate into strain-dependent macroscopic rheological properties is essential to understand the forces at play in important biological processes, such as wound healing and cancer metastasis, and to effectively design biomimetic synthetic materials.⁵

In this study, we consider a system composed of coarsegrained semiflexible filaments that diffusively self-assemble into a system-spanning network through the formation of permanent interfilament cross-links. We begin with randomly positioned free filaments with a specified coverage fraction p of "sticky" or linker-decorated sites. The linker coverage fraction serves as a proxy for the ratio of cross-linker and filament concentrations in a real system. Allowing diffusive motion to proceed, we add permanent cross-links (short elastic bonds, depicted in blue in Figure 1a) between sticky sites whose pairwise distance decreases beneath a designated cross-link formation distance. After the rate of diffusion-driven formation of new cross-links becomes sufficiently slow (see Section S4 in the Supporting Information), we stop the assembly process and permanently fix the topology of the network. In other words, any cross-links that have already formed remain permanent, while any sticky sites that have not formed crosslinks are permanently inactivated. We then analyze the structure of the fixed network, measuring the dependence of various structural features on the linker coverage fraction. An example network is shown in Figure 1a, and a movie depicting the assembly process is provided in the Supporting Information.

After fixing the network topology, we transition to the rheology stage, in which we observe the behavior of the network at steady state under constant simple shear strain γ . We obtain time series measurements of the thermally fluctuating shear stress $\sigma(\gamma,t)$ in the mechanically equilibrated state, as shown schematically in Figure 1b. Repeating these measurements over a range of strains for each set of input parameters, we calculate relevant elastic quantities such as the

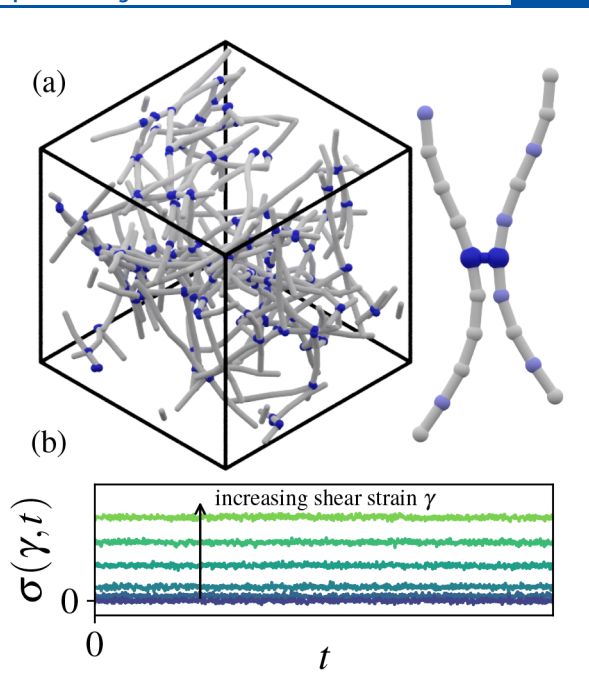


Figure 1. Model system and rheological approach. (a) Coarse-grained semiflexible filaments are decorated with randomly assigned sticky sites (light blue spheres in the image on the right) with coverage fraction p. When two sticky sites meet, they are connected by a permanent cross-link (royal blue dumbbell). Solutions of these filaments diffusively self-assemble into percolating disordered networks with macroscopic elasticity. (b) After the assembly process is stopped, the network topology remains fixed and the strain-dependent rheological properties are determined from the fluctuating shear stress $\sigma(\gamma, t)$ measured under a simple macroscopic shear strain γ .

differential shear modulus $K_{\rm eq}$ and the critical strain γ_c , at which the macroscopic system transitions between mechanical regimes dominated by bending and stretching. Appropriate physical parameters are chosen to enable comparison with previous experimental measurements of the elasticity of irreversibly cross-linked networks of F-actin, 49 an essential component of the cytoskeleton of eukaryotic cells. Using the same time series measurements, we then characterize the dynamics of stress-relaxation via time correlations in the stress fluctuations. Building upon recent work, ¹⁷ we demonstrate that the excess differential viscosity, a measure of energy dissipation reflected in a system's finite-temperature stress fluctuations, is directly proportional to the corresponding quasistatic, athermal differential nonaffinity, a measure of the rearrangement induced by a small strain perturbation in the quasistatic, athermal limit. Since in disordered networks the quasistatic nonaffinity is highly strain dependent and reaches a maximum at the critical strain, analogous behavior is expected in the excess differential viscosity and the slowest viscoelastic relaxation time. Our simulations confirm this expectation, providing crucial insight into potentially measurable effects of nonaffine fluctuations, which have generally proven challenging to experimentally quantify.

2. MODEL DEFINITION AND NETWORK ASSEMBLY

We imagine a system that begins as a solution of free semiflexible filaments covered to some extent with bound linker proteins that are capable of dimerizing to form permanent elastic cross-links. In experiments, the linker coverage could be controlled by varying the relative

concentrations of the cross-linking protein and filament monomer, as in ref 49. If the filament concentration and linker coverage in such a solution are sufficiently high, the formation of cross-links between diffusively migrating filaments eventually produces a macroscopic network.

To capture this behavior, we turn to a simplified computational model. We specify the number of filaments $N_{\rm f}$, filament length $l_{\rm f}$, and filament length density ρ , which together determine the size of the periodic simulation box, $L = (N_{\rm f} l_{\rm f}/\rho)^{1/3}$. To ensure that the (initially straight) filaments do not span the entire system, we require $L > l_f$ or equivalently $l_{\rm f} < \sqrt{N_{\rm f}/\rho}$. We also specify the number of evenly spaced nodes per filament, n, which determines the filament bond rest length $l_0 = l_f/(n-1)$. The total number of nodes in the system is then $N = N_t n$. We then designate a fraction p of the nodes, randomly chosen, as sticky or capable of forming a cross-link bond with another node of the same type. Cross-links are permanent bonds with a rest length $l_{0,cl}$ shorter than filament bonds. All bonds, including cross-links, are treated as harmonic springs with stretching stiffness μ , and harmonic bending interactions with stiffness $\kappa = k_B T l_p$ act between adjacent filament bonds. Here, $l_{\rm p}$ denotes the persistence length of the filament. In terms of the 3Ndimensional vector of node positions x, we write the elastic potential energy of this system as

$$U(\mathbf{x}) = \frac{\mu}{2} \sum_{ij} \frac{(l_{ij} - l_{ij,0})^2}{l_{ij,0}} + \frac{\kappa}{2} \sum_{ijk} \frac{(\theta_{ijk} - \theta_{ijk,0})^2}{l_{ijk,0}}$$
(1)

in which $l_{ij} = |\mathbf{x}_j - \mathbf{x}_i|$, θ_{ijk} is the angle between the bonds ij and jk, $l_{ijk} = (l_{ij} + l_{jk})/2$, and the subscript 0 denotes the rest values. The first sum is taken over all bonds ij, including crosslink bonds, and the second over all pairs of connected bonds ij and jk along the backbone of each filament. Because we consider cross-linked networks with very low filament volume fractions, we deem it acceptable to ignore steric interactions between filaments. Neglecting inertia, as is appropriate for the time scales studied here, the system obeys the overdamped Langevin equation, 51,52 such that the forces acting on all nodes satisfy

$$\mathbf{F}_{\mathrm{N}} + \mathbf{F}_{\mathrm{D}} + \mathbf{F}_{\mathrm{B}} = \mathbf{0} \tag{2}$$

in which the terms on the left represent the network forces, drag forces, and Brownian forces, respectively. The force due to the network is

$$\mathbf{F}_{\mathrm{N}} = -\frac{\partial U(\mathbf{x})}{\partial \mathbf{x}} \tag{3}$$

The nodes are subjected to a Stokes drag force

$$\mathbf{F}_{\mathrm{D}} = -\zeta \frac{\partial \mathbf{x}}{\partial t} \tag{4}$$

with drag coefficient $\zeta = 6\pi\eta_s a$ in which η_s is the solvent viscosity and a is an effective node radius of one-half the filament bond length, $a = l_0/2$. Finally, the Brownian force is

$$\mathbf{F}_{\mathrm{B}} = \sqrt{2\zeta k_{\mathrm{B}} T} \dot{\mathbf{w}} \tag{5}$$

in which each component of $\dot{\mathbf{w}}(t)$ is a Gaussian random variable with zero mean and unit variance. Equation 2 can be rewritten as

$$\frac{\partial \mathbf{x}}{\partial t} = -\frac{1}{\zeta} \frac{\partial U(\mathbf{x})}{\partial \mathbf{x}} + \sqrt{\frac{2k_{\rm B}T}{\zeta}} \dot{\mathbf{w}}(t)$$
(6)

During each time step in the assembly stage, we check whether the distance separating any pair of sticky nodes has decreased below a specified cross-link formation distance r_c , in which case we connect the two with a cross-link bond. Each sticky node can form a maximum of one cross-link, and connections between cross-links and filaments are treated as freely hinging. In other words, we do not include a bending potential between adjacent cross-link and filament bonds. We stop the assembly stage after a total time τ_a has elapsed. We find that $\tau_a = 6 \times 10^7 \Delta t$, corresponding to approximately 1 min in real units, is long enough for the rate of cross-link formation to become negligible (see Section S4 in the Supporting Information for further discussion). Note that cross-link formation does not take place after the assembly stage; during the rheology stage, described in the next section, the network topology remains fixed.

We note that the assembled networks are inevitably in a prestressed state, as the finite-temperature assembly process involves the formation of new constraints (cross-links) between filaments that are in fluctuating states of local bending, stretching, or compression. However, as we will see in the next section, the assembled networks clearly remain well within the bending-dominated linear elastic regime, indicating that the effects of this thermally induced prestress on network elasticity are insignificant.

After assembly, we analyze the structural features of each network. To determine the connectivity z or the average number of connections at each network junction, we consider a reduced version of the simulated network. Each pair of crosslinked nodes in the original network corresponds to a single node in the reduced network, and each filament section between two cross-linked nodes in the original network corresponds to an edge (see sketch in Figure S1 and further details in the Supporting Information, Section S1). Dangling ends, or filament sections in the original network connected to only one cross-link, are therefore neglected. This is a reasonable choice as dangling ends do not contribute to the elastic response of the network at zero frequency. We then calculate the connectivity from the number of edges n_{edges} and nodes n_{nodes} present in the reduced network structure as z = $2n_{\rm edges}/n_{\rm nodes}$.

We construct systems with filament length $l_{\rm f}=9~\mu{\rm m}$ and filament persistence length $l_{\rm p}=17~\mu{\rm m}$, chosen to approximate F-actin, with filament length per volume $\rho=2.6~\mu{\rm m}^{-2}$ (for F-actin, this corresponds to a concentration of $c_{\rm A}=1.6~\mu{\rm M}$). Additional parameters are specified in Table S1 (see Supporting Information). Unless otherwise stated, the measurements reported throughout this work are averaged over three randomly generated network samples, and error bars represent ± 1 standard deviation. All simulations are performed using the open source molecular dynamics simulation tool LAMMPS. S3

We first consider the effects of adjusting the cross-linker coverage fraction p on the assembled network structure. Varying p from 0.4 to 0.9, we find that the connectivity of the fully assembled network structures ranges from $z \in [2.8, 3.6]$, increasing monotonically with p (see Figure 2a). These values are similar to those measured for collagen and fibrin networks in previous experimental work. Next, we determine

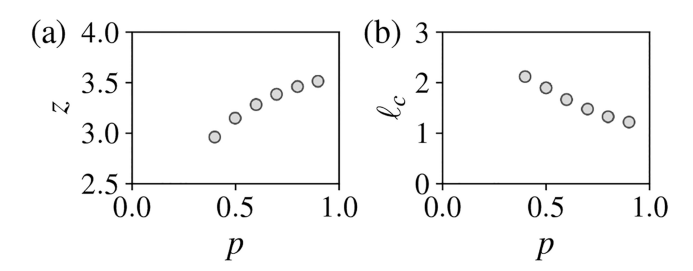


Figure 2. Linker coverage dependence of key structural characteristics of assembled networks. As the linker coverage fraction p increases, we observe (a) an increase in the average connectivity z and (b) a decrease in the average contour length between cross-links l_c .

the average intercross-link contour length $l_{\rm c}$, referring to the average distance between consecutive cross-links on each filament. We calculate $l_{\rm c}$ as the average length of the filament sections in the original network corresponding to the edges of the reduced network. As shown in Figure 2b, we find that $l_{\rm c}$ decreases monotonically with p.

3. NONLINEAR RHEOLOGY

After the assembly stage is halted, we proceed to the rheology stage, in which the strain-dependent steady-state viscoelastic properties of the system are measured via the time-dependent shear stress as the system fluctuates about the mechanically equilibrated state under a fixed shear strain. We impose a constant macroscopic simple shear strain γ using Lees–Edwards periodic boundary conditions and, using the conjugate gradient method, initially obtain the energy-minimizing configuration of the network, corresponding to the mechanically equilibrated state at T=0. Then, we evolve the system according to eq 6 at temperature T>0, specified in Table S1 of the Supporting Information, for a total run time $\tau_{\rm tot}=3\times10^7\Delta t$, discarding the first half of the trajectory to avoid initialization effects. For a given configuration of the system, we compute the instantaneous virial stress tensor

$$\sigma_{\alpha\beta} = \frac{1}{2V} \sum_{i>j} f_{ij\alpha} r_{ij\beta} \tag{7}$$

in which $\mathbf{r}_{ij} = \mathbf{x}_j - \mathbf{x}_i$ and \mathbf{f}_{ij} is the force acting on node i due to its interaction with node j. Because we will focus on macroscopic simple shear oriented along the x axis with gradient direction z, we now define $\sigma \equiv \sigma_{xz}$ to simplify notation. Once we have obtained a time series of the shear stress $\sigma(\gamma, t)$ at strain γ , we calculate the time-averaged shear stress $\langle \sigma(\gamma, t) \rangle_t$. After repeating this procedure over many strains in the interval $\gamma \in [0, 1]$, we compute the strain-dependent differential shear modulus

$$K_{\rm eq}(\gamma) = \frac{\partial \langle \sigma(\gamma, t) \rangle_t}{\partial \gamma} \tag{8}$$

which measures the apparent stiffness of the sample under macroscopic strain γ in response to an infinitesimal additional shear strain step. For sufficiently small strains, this yields the corresponding linear shear modulus, $G_0 = \lim_{\gamma \to 0} K_{\rm eq}(\gamma)$.

In Figure 3a and 3b, we plot the mean stress $\langle \sigma(\gamma,t) \rangle_t$ and the differential shear modulus $K_{\rm eq}$ as a function of strain for a single network sample with the parameters specified in Table S1 (see Supporting Information) and linker coverage fraction p = 0.9. We determine the critical strain γ_c , which indicates the transition between the bending-dominated and the stretching-

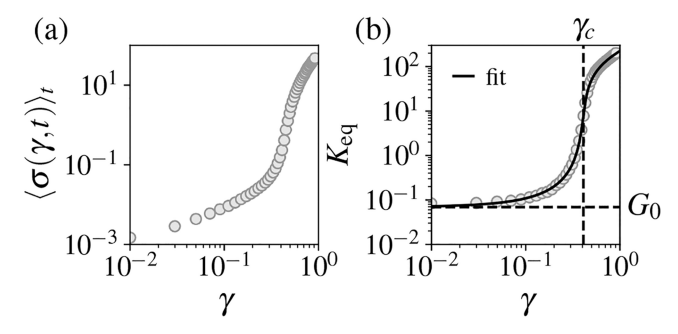


Figure 3. (a) Time-averaged shear stress $\langle \sigma(\gamma,t) \rangle_t$ as a function of applied shear strain γ for a single network sample with linker coverage fraction p=0.9. (b) Differential shear modulus $K_{\rm eq}=\partial \langle \sigma(\gamma,t) \rangle_t/\partial \gamma$. Linear shear modulus G_0 and critical strain γ_c are indicated by dashed lines, and solid line is a fit to the equation of state from ref 15, as described in the Supporting Information, Section S3.

dominated mechanical regimes, as the inflection point of the $\log K_{\rm eq}$ vs $\log \gamma$ curve. To avoid issues associated with differentiating noisy data, we can alternatively find G_0 and $\gamma_{\rm c}$ by fitting the entire $K_{\rm eq}$ vs γ curve to an Ising-like equation of state discussed in prior work, ¹⁵ as we describe in further detail in the Supporting Information, Section S3. Such a fit is shown in Figure 3b. For the data presented here, both methods effectively produce equivalent values of G_0 and γ_c .

In Figure 4, we report the strain dependence of the differential shear modulus for networks with varying linker

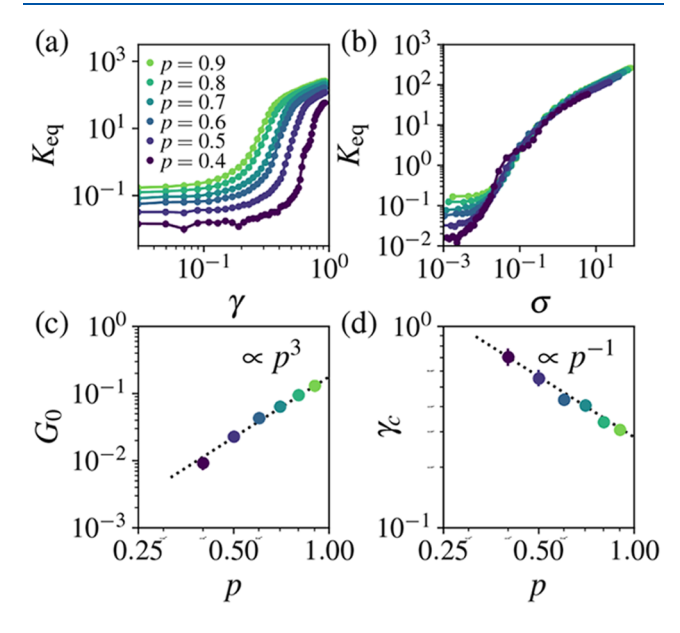


Figure 4. Effects of linker coverage on features of the linear and nonlinear stiffness in shear. Differential shear modulus $K_{\rm eq}$ for networks with varying linker coverage fraction p (a) as a function of strain and (b) as a function of shear stress. Increasing the linker coverage fraction p drives (c) an increase in the linear modulus $G_0 = \lim_{\gamma \to 0} K_0$ with $G_0 \propto p^3$ and (d) a decrease in the critical strain γ_c as $\gamma_c \propto p^{-1}$.

coverage fraction p. As p increases, the critical strain evidently decreases (stiffening occurs at lower applied strains) and the linear shear modulus increases. These observations qualitatively agree with the observed cross-linker concentration dependence of both the linear modulus G_0 and the rupture strain $\gamma_{\rm max}$ (which we expect to be proportional to γ_c) of F-

actin gels reported in ref 49 and with the connectivity dependence of the linear modulus and critical strain observed in spring network simulations.²⁰ The same differential shear modulus data are plotted in Figure 4b as a function of stress. The linear modulus G_0 and critical strain γ_c values extracted from these curves are plotted as functions of the linker coverage fraction p in Figure 4c and 4d, respectively. We find that each exhibits a power-law dependence on p, with $G_0 \propto p^3$ and $\gamma_c \propto p^{-1}$. In ref 49, in which the analogous quantity R (the ratio between the concentrations of actin and the cross-linking protein scruin) is varied, the authors report $G_0 \propto R^2$ and $\gamma_c \propto$ $R^{-0.6}$. These observations may be consistent with ours, provided that the linker coverage fraction in our system maps to the experimental cross-linker concentration ratio in ref 49 as $p \propto R^x$ with $x \approx 0.6$. Separately, the authors of ref 57 reported that for networks of actin filaments cross-linked by heavy meromyosin, $G_0 \propto R^{1.2}$ and $\gamma_{\rm c} \propto R^{-0.4}$, consistent with our observed dependence of both quantities on p if $x \approx 0.4$. However, meaningfully relating p and R will require further investigation. Here, for example, no two sticky sites on the same filament can reside closer than a distance l_0 (1 μ m with our parameters) from each other. This is obviously not the case in real F-actin networks.

In Figure 5a and 5b, we plot the same extracted linear shear modulus measurements as functions of the p-dependent structural quantities discussed in the previous section, the average network connectivity z and average intercross-link contour length $l_{\rm c}$. We observe an apparent power-law dependence of the linear shear modulus G_0 on the inter-

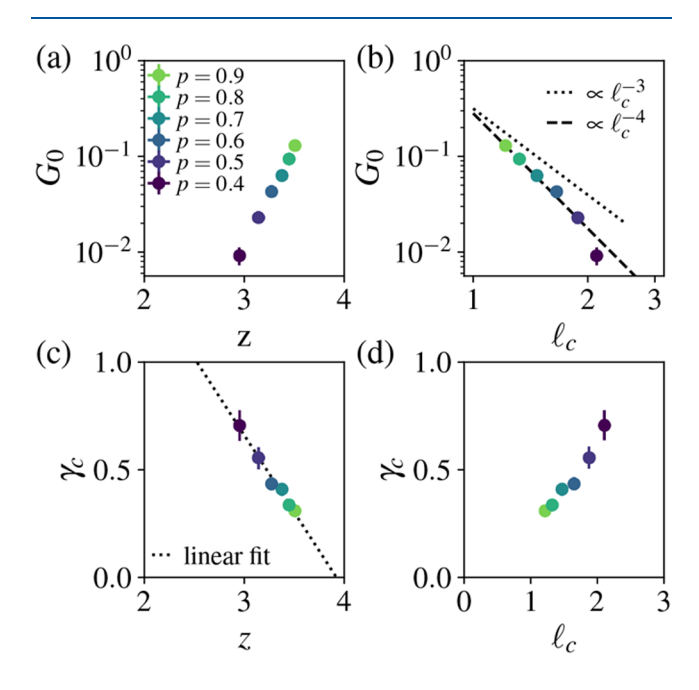


Figure 5. Linear shear modulus G_0 (a) increases dramatically with connectivity, shown here for systems with varying linker coverage fraction p, and (b) decreases with increasing average intercross-link contour length I_c . For small I_c (high p), we find $G_0 \propto I_c^{-\gamma}$ with $\gamma \approx 4$. Deviation from this scaling appears at higher values of I_c . (c) Critical strain γ_c , on the contrary, decreases approximately linearly with z. Linear fit suggests $\gamma_c \to 0$ as $z \to z^* \approx 4$, roughly consistent with the upper bound for z in the high cross-link density limit. (d) Critical strain increases approximately linearly with increasing average intercross-link contour length, $\gamma_c \propto I_c$.

cross-link contour length I_c , $G_0 \propto I_c^{-y}$, with decay exponent $y \approx$ 4. This appears to agree with the expected scaling of G_0 with I_c for an athermal network of stiff filaments. 25,58,59 However, it is important to note that our measurements cover less than a decade in l_c , so any agreement may be coincidental. We thus cannot rule out the $G_0 \propto I_c^{-3}$ scaling expected for a thermal semiflexible gel,60 although for our range of parameters the typical intercross-link contour lengths are presumably too small for bending modes to be properly resolved. Reliably measuring the scaling of G_0 with I_c in these systems will require further investigation in simulations with reduced coarse graining, i.e., smaller l_0/l_i , over a greater range of l_c . In Figure 5c, we plot the measured critical strain γ_c as a function of the connectivity. We find that for the range of parameters considered here, γ_c appears to exhibit a linear dependence on z with a best-fit intercept near $z^* \approx 4$, in apparent agreement with the upper limit of z for cross-linked networks with high cross-linking density. ²¹ It is crucial to note that the dependence of the critical strain on connectivity is known to be sensitive to certain details of the underlying network structure; for example, for short-filament networks with structures derived from 3D jammed sphere packings, the critical strain goes to zero precisely at the isostatic point, z = 6, and shows a distinctly nonlinear dependence on z far from the isostatic point. 17 In our networks, we expect the z intercept to depend on the filament length l_i and the bending rigidity κ_i which both necessarily influence the structure of the assembled network. While we similarly observe that the critical strain shows an apparent linear dependence on the average intercross-link contour length I_c (see Figure 5d), this too warrants further investigation.

Further information is contained in the fluctuations of the instantaneous stress about its average value 61

$$\delta\sigma(\gamma, t) = \sigma(\gamma, t) - \langle \sigma(\gamma, t) \rangle_{t} \tag{9}$$

from which we compute the stress fluctuation autocorrelation function

$$C(\gamma, \tau) = \frac{V}{k_{\rm B}T} \langle \delta \sigma(\gamma, t) \delta \sigma(\gamma, t + \tau) \rangle_{t}$$
(10)

which reveals useful details about the time dependence of energy dissipation. 62,63

In Figure 6a, we show representative $C(\gamma, \tau)$ data for a single sample (the same sample as in Figure 3) under applied strains below, near, and above the critical strain γ_c . We find that stress fluctuations decay slowly when the applied macroscopic strain is near γ_c in contrast to a much faster decay for strains below or above the critical regime. We can quantify this strain-dependent change in relaxation dynamics by integrating the shear stress autocorrelation function $C(\gamma, \tau)$ over a sufficiently long range of lag times τ . In practice, the range of lag times for which we can reliably estimate $C(\gamma, \tau)$ is limited by the simulation run time. Assuming $C(\gamma, \tau)$ is known for lag times below a maximum τ_{max} , we can estimate the system's slowest relaxation time as

$$\tau_{\rm R}(\gamma, \, \tau_{\rm max}) = \frac{\int_0^{\tau_{\rm max}} \tau C(\gamma, \, \tau) d\tau}{\int_0^{\tau_{\rm max}} C(\gamma, \, \tau) d\tau} \tag{11}$$

In the limit $\tau_{\text{max}} \to \infty$, this converges to the true slowest relaxation time $\tau_{\text{R,0}}(\gamma)$. In Figure 6b, we plot the apparent

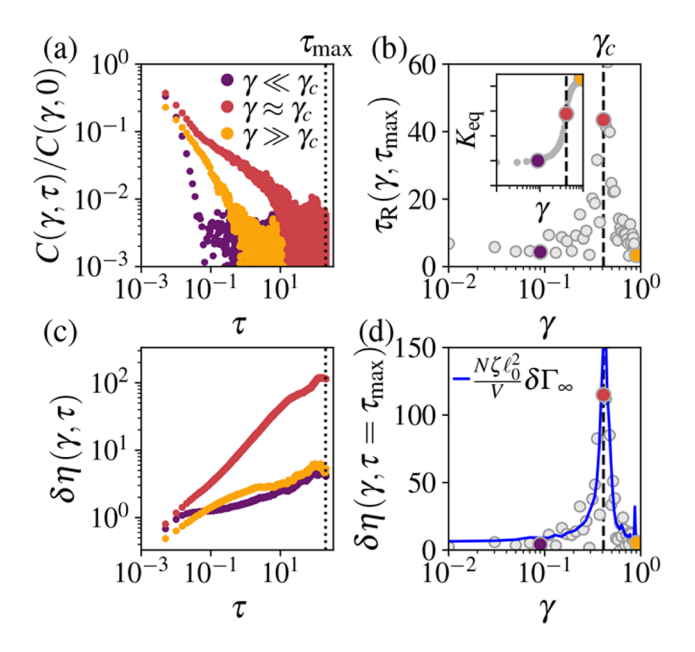


Figure 6. Relaxation of stress fluctuations slows dramatically near the critical strain as rearrangements become increasingly nonaffine. (a) Shear stress fluctuation autocorrelation function $C(\gamma, \tau)$ measured at representative strains below (purple), near (red), and above (orange) the critical strain γ_c (see the corresponding K_{eq} data in the inset of b) reveals this slowing, which is captured quantitatively by (b) a peak in the apparent slowest relaxation time τ_R (eq 11). These data correspond to the same sample as in Figure 3 (see inset), and labeled strains are indicated by the same colors in all panels. (c) At long lag times, the time-dependent apparent excess viscosity $\delta \eta(\gamma, \tau)$ calculated with eq 12 grows much larger near γ_c than elsewhere. This behavior is especially clear when (d) the apparent excess zero-shear viscosity $\delta \eta(\tau = \tau_{\text{max}})$ is plotted as a function of γ , revealing a peak at the p- (and thus z-) dependent critical strain. These observations are supported by independent measurements of the strain-dependent quasistatic, athermal differential nonaffinity $\delta\Gamma_{\infty}$, which is quantitatively related to $\delta \eta$ by eq 14 (solid blue line).

slowest relaxation time τ_R for the same system, with marker colors indicating the strains plotted in Figure 6a. Note that the corresponding stiffening curve from Figure 3 is also shown in the inset. We observe that τ_R grows substantially as the critical strain γ_c is approached from either side, reaching a maximum at γ_c . In fact, we see consistent behavior, that is, growth of the slowest relaxation time by an order of magnitude or more with a peak at p-dependent critical strain γ_c in networks throughout the range of p considered. This is shown in Figure 7d, in which the applied strain is normalized by the p-dependent critical strain γ_c revealing maxima in τ_R at $\gamma/\gamma_c = 1$ for all p.

The stress fluctuation autocorrelation function is also related to the system's lag-dependent excess differential viscosity $\delta\eta(\gamma, \tau) \equiv \eta(\gamma, \tau) - \eta_s$ measured at strain γ

$$\delta\eta(\gamma,\,\tau) = \int_0^\tau C(\gamma,\,\tau')\mathrm{d}\tau' \tag{12}$$

which we plot in Figure 6c for the same labeled strain values. It is clear that $\delta\eta(\gamma,\tau)$ grows far more dramatically near the critical strain than elsewhere. In recent work, ¹⁷ it was suggested that the low-frequency or "zero-shear" excess differential viscosity $\delta\eta_0(\gamma) = \lim_{\tau \to \infty} \delta\eta(\gamma,\tau)$ of prestrained disordered networks is controlled by nonaffinity. Specifically, $\delta\eta_0$ was shown to be related to the quasistatic, athermal differential nonaffinity $\delta\Gamma_{\infty}(\gamma)$, defined as

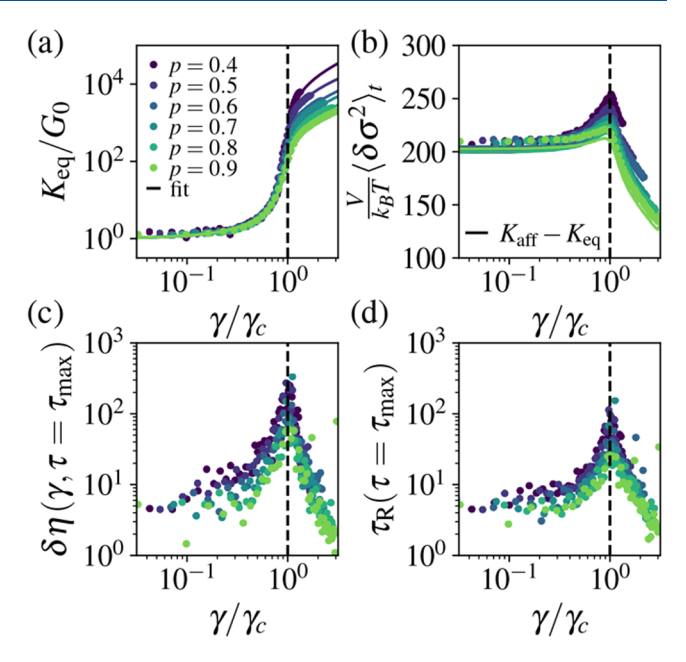


Figure 7. Shared features of stiffening and slowing down at the structure-dependent critical strain. (a) For networks with varying cross-linker coverage fraction p, the stiffening regime of the normalized differential shear modulus K/G_0 collapses onto a single curve when plotted vs γ/γ_c . Lines correspond to fits to the equation of state described in ref 15 (see Supporting Information, Section S3), and associated fit parameters are plotted as a function of p in Figure S2. (b) Mean squared stress fluctuations $\langle \delta \sigma(\gamma, t)^2 \rangle_t$ are largest at the p- (and thus z-) dependent critical strain. Solid lines correspond to the difference between the measured strain-dependent affine and the equilibrium differential shear moduli, $K_{\rm aff}$ and $K_{\rm eq}$, according to eq 16. Both the (a) apparent excess zero-shear viscosity $\delta \eta$ and (b) apparent slowest relaxation time $\tau_{\rm R}$ also exhibit large peaks at the p-dependent critical strain γ_c .

$$\delta\Gamma_{\infty}(\gamma) = \lim_{\delta\gamma \to 0} \frac{1}{N I_0^2 \delta \gamma^2} \sum_i |\delta \mathbf{x}_i^{\text{NA}}|^2$$
(13)

in which the sum is taken over all network nodes and the vector $\delta \mathbf{x}_i^{\mathrm{NA}}$ represents the nonaffine component of the displacement vector of node i under a macroscopic, quasistatically applied strain step $\delta \gamma$. The viscosity—nonaffinity relationship in ref 17 can be stated concisely as

$$\delta\eta_0(\gamma) = \frac{N}{V} \zeta I_0^2 \delta \Gamma_{\infty}(\gamma) \tag{14}$$

The left-hand side of eq 14 reflects the dynamics of the stress fluctuations at finite temperature, while the right side reflects the heterogeneous nature of the strictly quasistatic deformation field, which can be obtained by comparing energy-minimized T = 0 system configurations under varying applied γ .

Simulations have suggested that for disordered filament networks, the differential nonaffinity generically reaches a maximum at the structure-dependent critical strain, 64,65 at which the system macroscopically transitions between bending-dominated (or floppy, for $\kappa=0$) and stretching-dominated regimes. Thus, according to eq 14, we should generically see a proportional peak in the excess differential viscosity at γ_c . Testing this prediction requires measuring the quasistatic, athermal differential nonaffinity. To do so, for a given network at strain γ , we first obtain the energy-minimizing configuration at T=0 using the conjugate gradient method.

To this configuration, we then apply a small additional strain step d $\gamma=0.01$, after which we repeat the energy minimization procedure. Comparing the positions in the energy-minimizing configurations at γ and $\gamma+d\gamma$, we compute the quasistatic differential nonaffinity $\delta\Gamma_{\infty}$ using eq 13. In Figure 6d, we plot $\delta\Gamma_{\infty}$ along with the apparent excess differential zero-shear viscosity for the same system, demonstrating excellent agreement with eq 14. To demonstrate that this behavior is preserved as the structure is varied, we show in Figure 7c that a clear peak in $\delta\eta$ occurs at $\gamma/\gamma_c=1$ over the entire range of p considered.

We can also use the stress fluctuations to determine the differential relaxation modulus ⁶⁶

$$K(\gamma, \tau) = K_{eq}(\gamma) + C(\gamma, \tau)$$
(15)

which quantifies the time-dependent apparent stiffness of the system at prestrain γ in response to an instantaneous additional strain step. For sufficiently short times, the differential relaxation modulus approaches an upper limit of $\lim_{\tau \to 0} K(\gamma, \tau) = K_{\rm aff}(\gamma)$, corresponding to the apparent stiffness of the energy-minimized, athermal equivalent of the system at strain γ under an instantaneous, homogeneous infinitesimal shear strain step. Consequently, the equilibrium stiffness of the system under applied strain γ is simply $K_{\rm aff}(\gamma)$ reduced by $C(\gamma, 0)^{61,69,70}$ or equivalently

$$K_{\rm eq}(\gamma) = K_{\rm aff}(\gamma) - \frac{V}{k_{\rm B}T} \langle (\delta \sigma(\gamma, t))^2 \rangle_t$$
 (16)

We find that this relationship provides a useful estimate of the mean squared stress fluctuations, as shown in Figure 7b, and we observe that the mean squared stress fluctuations robustly reach a maximum at $\gamma/\gamma_c = 1$.

4. DISCUSSION AND CONCLUSIONS

We have investigated the assembly and mechanical testing of disordered networks of cross-linked semiflexible polymers via Brownian dynamics simulations. Such networks serve as essential mechanical constituents of a wide variety of biological materials spanning many length scales. We explored the structural and rheological consequences of varying the cross-linker coverage fraction p, an analog of the experimental ratio between the concentrations of cross-linker and filament proteins. Using physical parameters intended to mimic the cytoskeletal polymer F-actin, we measured the effects of increasing the linker coverage fraction p on the average connectivity z of self-assembled networks, observing a corresponding increase in connectivity between $z \in [2.8, 3.6]$.

We then investigated the relationship between these connectivity changes and the associated changes in the strain-dependent rheological properties of the assembled networks, obtaining extended time series measurements of fluctuating shear stress $\sigma(\gamma, t)$ for systems held under fixed shear strain γ . Analyzing many such trajectories gathered over a range of applied strains γ , we computed the strain-dependent differential shear modulus $K_{\rm eq}$ from which we extracted both the linear shear modulus G_0 and the critical strain γ_c . We described the dependence of these quantities on the cross-linker coverage fraction p, demonstrating qualitative agreement with the experimentally observed dependence of the same quantities on the cross-linker concentration ratio R reported in ref 49. Specifically, we found that increasing p produces inherently stiffer networks (having an increased linear shear

modulus G_0) that simultaneously exhibit an earlier tendency to strain stiffen (having a lower critical strain γ_c). Drawing comparisons between the scaling of both G_0 and γ_c with p and the analogous experimentally observed scaling of the same quantities with R, we suggested a simple power-law relationship between p and R. We then described the apparent dependence of these elastic features on the p-dependent structural quantities z and l_c , notably showing that the critical strain decreases linearly with z. A linear fit suggests that γ_c approaches 0 as the connectivity z approaches a limiting value $z^* \rightarrow z_c$ near 4, the theoretical upper bound for z at high cross-linking density.

We then extended our observations beyond strictly elastic properties by analyzing the stress fluctuation autocorrelation function $C(\gamma, \tau)$, which revealed the development of extremely slow dynamics in systems subjected to applied shear strains near the critical strain γ_c . From $C(\gamma, \tau)$, we obtained estimates of the slowest relaxation time $au_{R,0}$ and the excess differential zero-shear viscosity $\delta\eta_0$, both of which we showed are consistently maximized at the p-dependent critical strain, irrespective of the details of the underlying network. Building upon results from ref 17, we demonstrated that the excess differential viscosity in these finite-temperature systems is quantitatively controlled by the athermal quasistatic differential nonaffinity $\delta\Gamma_{\infty}$, a measure of the inherent tendency of the strained network to deform heterogeneously. Importantly, our results suggest that one should expect measurable dynamical signatures of transition-associated nonaffine fluctuations to appear in semiflexible polymer networks with biologically relevant elastic properties, e.g., those of the F-actin cytoskeleton, under physiologically relevant applied strains. In other words, one should generically expect to observe slowing stress-relaxation in biopolymer networks at prestrain levels near the critical strain γ_c , marking the macroscopic transition between bending-dominated and stretching-dominated elasticity. Since γ_c is controlled by the average connectivity z, which is controlled in turn by the availability of cross-linking sites (here, p), our results suggest a route to experimentally control the strain dependence of major features of both network elasticity and stress-relaxation dynamics.

In future work, it would be prudent to explore how the behavior we observe near the critical strain might differ in networks with linkers capable of either breaking under sufficient tension 43,46,71 or transiently binding and unbinding. 72,73 In such systems, we anticipate a rich interplay between the slow relaxations associated with nonaffine rearrangements and the additional dynamics of network remodeling and fracture.

ASSOCIATED CONTENT

SUPPORTING Information

The Supporting Information is available free of charge at https://pubs.acs.org/doi/10.1021/acs.jpcb.2c05439.

Sample animation of network assembly (MP4)

Simulation parameters; connectivity and intercross-link contour length calculation details; discussion of fitting the differential shear modulus; discussion of the stopping criterion for network assembly (PDF)

AUTHOR INFORMATION

Corresponding Author

Jordan L. Shivers — Center for Theoretical Biological Physics, Rice University, Houston, Texas 77005, United States; Department of Chemical and Biomolecular Engineering, Rice University, Houston, Texas 77005, United States;

orcid.org/0000-0002-3884-1708; Email: jshivers@uchicago.edu

Authors

Saamiya Syed — College of Technology, University of Houston, Houston, Texas 77204, United States; Center for Theoretical Biological Physics, Rice University, Houston, Texas 77005, United States; orcid.org/0000-0002-6635-9919

Fred C. MacKintosh — Center for Theoretical Biological Physics, Rice University, Houston, Texas 77005, United States; Department of Chemical and Biomolecular Engineering, Department of Chemistry, and Department of Physics & Astronomy, Rice University, Houston, Texas 77005, United States; orcid.org/0000-0002-2607-9541

Complete contact information is available at: https://pubs.acs.org/10.1021/acs.jpcb.2c05439

Notes

The authors declare no competing financial interest.

ACKNOWLEDGMENTS

This study was supported in part by the National Science Foundation Division of Materials Research (Grant No. DMR-1826623) and the National Science Foundation Center for Theoretical Biological Physics (Grant No. PHY-2019745). This work began as a summer Research Experience for Undergraduates (REU) project supported by the Frontiers in Science (FIS) program of the Center for Theoretical Biological Physics.

REFERENCES

- (1) Burla, F.; Mulla, Y.; Vos, B. E.; Aufderhorst-Roberts, A.; Koenderink, G. H. From mechanical resilience to active material properties in biopolymer networks. *Nature Reviews Physics* **2019**, *1*, 249–263.
- (2) Janmey, P. A. Mechanical properties of cytoskeletal polymers. *Curr. Opin. Cell Biol.* **1991**, *3*, 4–11.
- (3) Tyznik, S.; Notbohm, J. Length scale dependent elasticity in random three-dimensional fiber networks. *Mech. Mater.* **2019**, *138*, 103155.
- (4) Proestaki, M.; Ogren, A.; Burkel, B.; Notbohm, J. Modulus of Fibrous Collagen at the Length Scale of a Cell. *Experimental Mechanics* **2019**, *59*, 1323–1334.
- (5) Onck, P. R.; Koeman, T.; van Dillen, T.; van der Giessen, E. Alternative explanation of stiffening in cross-linked semiflexible networks. *Phys. Rev. Lett.* **2005**, 95, 178102.
- (6) Picu, R. C.; Deogekar, S.; Islam, M. R. Poisson's Contraction and Fiber Kinematics in Tissue: Insight From Collagen Network Simulations. *J. Biomech. Eng.* **2018**, *140*, 021002.
- (7) Ban, E.; Wang, H.; Franklin, J. M.; Liphardt, J. T.; Janmey, P. A.; Shenoy, V. B. Strong triaxial coupling and anomalous Poisson effect in collagen networks. *Proc. Natl. Acad. Sci. U. S. A.* **2019**, *116*, 6790–6799.
- (8) Notbohm, J.; Lesman, A.; Rosakis, P.; Tirrell, D. A.; Ravichandran, G. Microbuckling of fibrin provides a mechanism for cell mechanosensing. *Journal of The Royal Society Interface* **2015**, 12, 20150320.

- (9) Wang, H.; Abhilash, A. S.; Chen, C. S.; Wells, R. G.; Shenoy, V. B. Long-range force transmission in fibrous matrices enabled by tension-driven alignment of fibers. *Biophys. J.* **2014**, *107*, 2592–2603.
- (10) Han, Y. L.; Ronceray, P.; Xu, G.; Malandrino, A.; Kamm, R. D.; Lenz, M.; Broedersz, C. P.; Guo, M. Cell contraction induces long-ranged stress stiffening in the extracellular matrix. *Proc. Natl. Acad. Sci. U. S. A.* **2018**, *115*, 4075–4080.
- (11) Alisafaei, F.; Chen, X.; Leahy, T.; Janmey, P. A.; Shenoy, V. B. Long-range mechanical signaling in biological systems. *Soft Matter* **2021**, *17*, 241–253.
- (12) Grill, M. J.; Kernes, J.; Slepukhin, V. M.; Wall, W. A.; Levine, A. J. Directed force propagation in semiflexible networks. *Soft Matter* **2021**, *17*, 10223–10241.
- (13) Huxley, H. E. The Mechanism of Muscular Contraction. *Science* **1969**, *164*, 1356–1366.
- (14) Gunst, S. J.; Fredberg, J. J. The first three minutes: smooth muscle contraction, cytoskeletal events, and soft glasses. *J. Appl. Physiol.* **2003**, 95, 413–425.
- (15) Sharma, A.; Licup, A. J.; Jansen, K. A.; Rens, R.; Sheinman, M.; Koenderink, G. H.; MacKintosh, F. C. Strain-controlled criticality governs the nonlinear mechanics of fibre networks. *Nat. Phys.* **2016**, *12*, 584–587.
- (16) Jansen, K. A.; Licup, A. J.; Sharma, A.; Rens, R.; MacKintosh, F. C.; Koenderink, G. H. The Role of Network Architecture in Collagen Mechanics. *Biophys. J.* **2018**, *114*, 2665–2678.
- (17) Shivers, J. L.; Sharma, A.; MacKintosh, F. C. Nonaffinity controls critical slowing down and rheology near the onset of rigidity. *arXiv*:2203.04891 **2022** DOI: 10.48550/arXiv.2203.04891.
- (18) Andreotti, B.; Barrat, J.-L.; Heussinger, C. Shear Flow of Non-Brownian Suspensions Close to Jamming. *Phys. Rev. Lett.* **2012**, *109*, 105901.
- (19) Lerner, E.; Düring, G.; Wyart, M. A unified framework for non-Brownian suspension flows and soft amorphous solids. *Proc. Natl. Acad. Sci. U. S. A.* **2012**, *109*, 4798–4803.
- (20) Wyart, M.; Liang, H.; Kabla, A.; Mahadevan, L. Elasticity of floppy and stiff random networks. *Phys. Rev. Lett.* **2008**, *101*, 215501.
- (21) Broedersz, C. P.; Sheinman, M.; MacKintosh, F. C. Filament-length-controlled elasticity in 3D fiber networks. *Phys. Rev. Lett.* **2012**, 108, 078102.
- (22) Picu, R. C. Mechanics of random fiber networks—a review. *Soft Matter* **2011**, *7*, 6768–6785.
- (23) Carrillo, J.-M. Y.; MacKintosh, F. C.; Dobrynin, A. V. Nonlinear Elasticity: From Single Chain to Networks and Gels. *Macromolecules* **2013**, *46*, 3679–3692.
- (24) Freedman, S. L.; Banerjee, S.; Hocky, G. M.; Dinner, A. R. A Versatile Framework for Simulating the Dynamic Mechanical Structure of Cytoskeletal Networks. *Biophys. J.* **2017**, *113*, 448–460.
- (25) Huisman, E. M.; van Dillen, T.; Onck, P. R.; Van der Giessen, E. Three-Dimensional Cross-Linked F-Actin Networks: Relation between Network Architecture and Mechanical Behavior. *Phys. Rev. Lett.* **2007**, *99*, 208103.
- (26) Kim, T.; Hwang, W.; Kamm, R. D. Computational Analysis of a Cross-linked Actin-like Network. *Experimental Mechanics* **2009**, 49, 91–104.
- (27) Dobrynin, A. V.; Carrillo, J. M. Y. Universality in nonlinear elasticity of biological and polymeric networks and gels. *Macromolecules* **2011**, *44*, 140–146.
- (28) Müller, K. W.; Bruinsma, R. F.; Lieleg, O.; Bausch, A. R.; Wall, W. A.; Levine, A. J. Rheology of Semiflexible Bundle Networks with Transient Linkers. *Phys. Rev. Lett.* **2014**, *112*, 238102.
- (29) Müller, K. W.; Meier, C.; Wall, W. A. Resolution of sub-element length scales in Brownian dynamics simulations of biopolymer networks with geometrically exact beam finite elements. *I. Comput. Phys.* **2015**, 303, 185–202.
- (30) Żagar, G.; Onck, P. R.; van der Giessen, E. Two Fundamental Mechanisms Govern the Stiffening of Cross-linked Networks. *Biophys. J.* **2015**, *108*, 1470–1479.

- (31) DeBenedictis, E. P.; Zhang, Y.; Keten, S. Structure and Mechanics of Bundled Semiflexible Polymer Networks. *Macromolecules* **2020**, *53*, 6123–6134.
- (32) Huisman, E. M.; Storm, C.; Barkema, G. T. Monte Carlo study of multiply crosslinked semiflexible polymer networks. *Phys. Rev. E* **2008**, *78*, 051801.
- (33) Lindström, S. B.; Vader, D. A.; Kulachenko, A.; Weitz, D. A. Biopolymer network geometries: Characterization, regeneration, and elastic properties. *Phys. Rev. E* **2010**, 82, 051905.
- (34) Huisman, E. M.; Lubensky, T. C. Internal Stresses, Normal Modes, and Nonaffinity in Three-Dimensional Biopolymer Networks. *Phys. Rev. Lett.* **2011**, *106*, 088301.
- (35) Huisman, E. M.; Storm, C.; Barkema, G. T. Frequency-dependent stiffening of semiflexible networks: A dynamical nonaffine to affine transition. *Phys. Rev. E* **2010**, 82, 061902.
- (36) Lindström, S. B.; Kulachenko, A.; Jawerth, L. M.; Vader, D. A. Finite-strain, finite-size mechanics of rigidly cross-linked biopolymer networks. *Soft Matter* **2013**, *9*, 7302–7313.
- (37) Amuasi, H. E.; Heussinger, C.; Vink, R. L.; Zippelius, A. Nonlinear and heterogeneous elasticity of multiply-crosslinked biopolymer networks. *New J. Phys.* **2015**, *17*, 083035.
- (38) Vermeulen, M. F.; Bose, A.; Storm, C.; Ellenbroek, W. G. Geometry and the onset of rigidity in a disordered network. *Phys. Rev. E* **2017**, *96*, 053003.
- (39) Rens, R.; Villarroel, C.; Düring, G.; Lerner, E. Micromechanical theory of strain stiffening of biopolymer networks. *Phys. Rev. E* **2018**, 98. 62411.
- (40) Merkel, M.; Baumgarten, K.; Tighe, B. P.; Manning, M. L. A minimal-length approach unifies rigidity in underconstrained materials. *Proc. Natl. Acad. Sci. U. S. A.* **2019**, *116*, 6560–6568.
- (41) Shivers, J. L.; Feng, J.; Sharma, A.; MacKintosh, F. C. Normal stress anisotropy and marginal stability in athermal elastic networks. *Soft Matter* **2019**, *15*, 1666–1675.
- (42) Shivers, J. L.; Arzash, S.; MacKintosh, F. C. Nonlinear Poisson Effect Governed by a Mechanical Critical Transition. *Phys. Rev. Lett.* **2020**, 124, 038002.
- (43) Burla, F.; Dussi, S.; Martinez-Torres, C.; Tauber, J.; van der Gucht, J.; Koenderink, G. H. Connectivity and plasticity determine collagen network fracture. *Proc. Natl. Acad. Sci. U.S.A.* **2020**, *117*, 8326–8334.
- (44) Burla, F.; Tauber, J.; Dussi, S.; van der Gucht, J.; Koenderink, G. H. Stress management in composite biopolymer networks. *Nat. Phys.* **2019**, *15*, 549–553.
- (45) Dussi, S.; Tauber, J.; van der Gucht, J. Athermal Fracture of Elastic Networks: How Rigidity Challenges the Unavoidable Size-Induced Brittleness. *Phys. Rev. Lett.* **2020**, *124*, 018002.
- (46) Tauber, J.; van der Gucht, J.; Dussi, S. Stretchy and disordered: Toward understanding fracture in soft network materials via mesoscopic computer simulations. J. Chem. Phys. 2022, 156, 160901.
- (47) Broedersz, C. P.; MacKintosh, F. C. Modeling semiflexible polymer networks. *Rev. Mod. Phys.* **2014**, *86*, 995–1036.
- (48) Piechocka, I. K.; Jansen, K. A.; Broedersz, C. P.; Kurniawan, N. A.; MacKintosh, F. C.; Koenderink, G. H. Multi-scale strain-stiffening of semiflexible bundle networks. *Soft Matter* **2016**, *12*, 2145–2156.
- (49) Gardel, M. L.; Shin, J. H.; MacKintosh, F. C.; Mahadevan, L.; Matsudaira, P.; Weitz, D. A. Elastic Behavior of Cross-Linked and Bundled Actin Networks. *Science* **2004**, *304*, 1301–1305.
- (50) Fernandez-Castano Romera, M.; Lafleur, R. P. M.; Guibert, C.; Voets, I. K.; Storm, C.; Sijbesma, R. P. Strain Stiffening Hydrogels through Self-Assembly and Covalent Fixation of Semi-Flexible Fibers. *Angew. Chem., Int. Ed.* **2017**, *56*, 8771–8775.
- (51) Allen, M. P.; Tildesley, D. J. Computer Simulation of Liquids; Oxford University Press, 2017.
- (52) Frenkel, D.; Smit, B. Understanding molecular simulation: from algorithms to applications, 2nd ed.; Computational Science Series 1; Academic Press: San Diego, CA, 2002.
- (53) Thompson, A. P.; Åktulga, H. M.; Berger, R.; Bolintineanu, D. S.; Brown, W. M.; Crozier, P. S.; in 't Veld, P. J.; Kohlmeyer, A.; Moore, S. G.; Nguyen, T. D.; et al. LAMMPS a flexible simulation

- tool for particle-based materials modeling at the atomic, meso, and continuum scales. Comput. Phys. Commun. 2022, 271, 108171.
- (54) Beroz, F.; Jawerth, L. M.; Münster, S.; Weitz, D. A.; Broedersz, C. P.; Wingreen, N. S. Physical limits to biomechanical sensing in disordered fibre networks. *Nat. Commun.* **2017**, *8*, 16096.
- (55) Xia, J.; Cai, L.-H.; Wu, H.; MacKintosh, F. C.; Weitz, D. A. Anomalous mechanics of Zn2+-modified fibrin networks. *Proc. Natl. Acad. Sci. U. S. A.* **2021**, *118*, No. e2020541118.
- (56) Lees, A. W.; Edwards, S. F. The computer study of transport processes under extreme conditions. *Journal of Physics C: Solid State Physics* 1972, 5, 1921–1928.
- (57) Tharmann, R.; Claessens, M. M. A. E.; Bausch, A. R. Viscoelasticity of Isotropically Cross-Linked Actin Networks. *Phys. Rev. Lett.* **2007**, *98*, 88103.
- (58) Satcher, R. L.; Dewey, C. F. Theoretical estimates of mechanical properties of the endothelial cell cytoskeleton. *Biophys. J.* **1996**, *71*, 109–18.
- (59) Gibson, L. J.; Ashby, M. F. Cellular Solids: Structure and Properties, 2nd ed.; Cambridge Solid State Science Series; Cambridge University Press, 1997.
- (60) MacKintosh, F. C.; Kas, J.; Janmey, P. A. Elasticity of semiflexible biopolymer networks. *Phys. Rev. Lett.* **1995**, *75*, 4425–4428
- (61) Wittmer, J. P.; Xu, H.; Polińska, P.; Weysser, F.; Baschnagel, J. Shear modulus of simulated glass-forming model systems: Effects of boundary condition, temperature, and sampling time. *J. Chem. Phys.* **2013**, *138*, 12A533.
- (62) Wittmer, J.; Xu, H.; Benzerara, O.; Baschnagel, J. Fluctuation-dissipation relation between shear stress relaxation modulus and shear stress autocorrelation function revisited. *Mol. Phys.* **2015**, *113*, 2881–2893.
- (63) Wittmer, J. P.; Xu, H.; Baschnagel, J. Shear-stress relaxation and ensemble transformation of shear-stress autocorrelation functions. *Phys. Rev. E* **2015**, *91*, 022107.
- (64) Rens, R. Nonlinear elastic behavior of branched networks: Rapid strain stiffening as a critical phenomenon. Ph.D. Thesis, University of Amsterdam, 2014.
- (65) Sharma, A.; Licup, A. J.; Rens, R.; Vahabi, M.; Jansen, K. A.; Koenderink, G. H.; MacKintosh, F. C. Strain-driven criticality underlies nonlinear mechanics of fibrous networks. *Phys. Rev. E* **2016**, *94*, 042407.
- (66) Wittmer, J. P.; Kriuchevskyi, I.; Baschnagel, J.; Xu, H. Shear-strain and shear-stress fluctuations in generalized Gaussian ensemble simulations of isotropic elastic networks. *Eur. Phys. J. B* **2015**, *88*, 242.
- (67) Rubinstein, M.; Colby, R. Polymer Physics; Oxford University Press, 2006.
- (68) Doi, M.; Edwards, S. F. The Theory of Polymer Dynamics; Oxford University Press, 1988.
- (69) Squire, D. R.; Holt, A. C.; Hoover, W. G. Isothermal elastic constants for argon. Theory and Monte Carlo calculations. *Physica* **1969**, 42, 388–397.
- (70) Lutsko, J. F. Generalized expressions for the calculation of elastic constants by computer simulation. *J. Appl. Phys.* **1989**, *65*, 2991–2997.
- (71) Lwin, P.; Sindermann, A.; Sutter, L.; Wyse Jackson, T.; Bonassar, L.; Cohen, I.; Das, M. Rigidity and fracture of biopolymer double networks. *Soft Matter* **2022**, *18*, 322–327.
- (72) Amuasi, H. E.; Fischer, A.; Zippelius, A.; Heussinger, C. Linear rheology of reversibly cross-linked biopolymer networks. *J. Chem. Phys.* **2018**, *149*, 084902.
- (73) Scheff, D. R.; Redford, S. A.; Lorpaiboon, C.; Majumdar, S.; Dinner, A. R.; Gardel, M. L. Actin filament alignment causes mechanical hysteresis in cross-linked networks. *Soft Matter* **2021**, *17*, 5499–5507.